

Maxwell's lesser demon

Stella Seah,¹ Stefan Nimmrichter,² and Valerio Scarani^{1,3}

¹*Department of Physics, National University of Singapore, 2 Science Drive 3, Singapore 117542, Singapore*

²*Max Planck Institute for the Science of Light, Staudtstraße 2, 91058 Erlangen, Germany*

³*Centre for Quantum Technologies, National University of Singapore, 3 Science Drive 2, Singapore 117543, Singapore*

(Dated: August 28, 2019)

We discuss a self-contained spin-boson model for a measurement-driven engine, in which a demon generates work from random thermal excitations of a quantum spin via measurement and feedback control. Instead of granting it full direct access to the spin state and to Landauer's erasure strokes for optimal performance, we restrict this lesser demon's action to pointer measurements, i.e. random or continuous interrogations of a damped mechanical oscillator that assumes macroscopically distinct positions depending on the spin state. The engine could reach simultaneously high output powers and efficiencies and can operate in temperature regimes where quantum Otto engines would fail.

Conventionally, thermal machines operate through the interaction of a working medium with hot and cold reservoirs. In the context of quantum thermodynamics, interest has been raised in finding non-thermal resources such as coherence [1–5], squeezed baths [6–8] or measurement channels [9–12] that could induce advantages to standard thermal machines.

Specifically, the role of measurement in relation to thermodynamics and information flow has been studied rigorously. For example, models of thermal machines facilitated by Maxwell's demon – an external agent that acquires information of the system and performs appropriate feedback – have been proposed in order to provide accurate thermodynamic description of information flow [13–18]. More recently, a measurement channel has been deemed a source of “quantum heat” [9] due to the increased entropy following a measurement, which could be exploited for both cooling [11] and work extraction [10, 12, 19, 20]. However, proper treatment of actual erasure cost of pointers [21–23] as well as the interpretation of incoherent measurement schemes as a form of heat *and* work exchange [24–26] still remain a contentious topic for such measurement-based thermal machines.

In this paper, we investigate the role of measurement by considering a self-contained engine built from the standard ingredients (hot and cold reservoirs and a working medium) as well as an embedded pointer, modelled by a damped mechanical degree of freedom. In contrast to regular Maxwell-demon type engines where the demon has access to the state of the working medium and stores it in its memory, we restrict our demon's access to the pointer only, i.e. work can *only* be extracted from the medium by reading off the pointer position and applying appropriate feedback. We show that such a setup generates a new type of engine with features different from standard quantum engines. In particular, we see that the typical trade-off between work and efficiency is absent and it is possible to attain simultaneous high powers and efficiencies. The regime of operation is also generally wider than a typical Otto engine. More fundamentally, our proposed autonomous scheme serves as a platform to revisit the definitions of work and heat in a measurement-

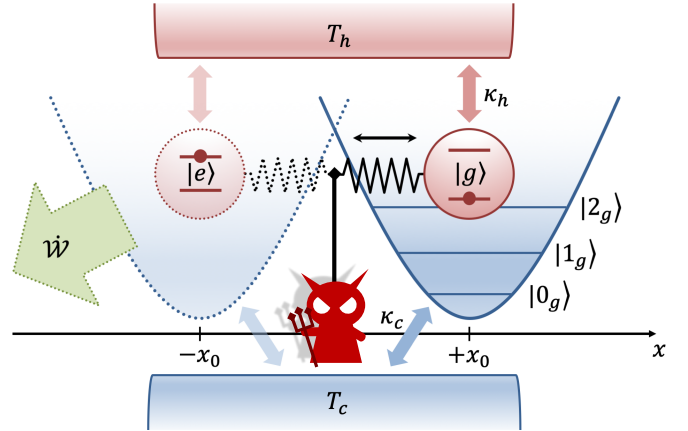


FIG. 1. Sketch of the demon system consisting of a qubit (working medium) and a harmonic oscillator (pointer). The qubit can be thermally excited by a hot bath at the rate κ_h and temperature T_h , and it displaces the equilibrium position of the pointer to $\pm x_0$ depending on its state. A cold bath of temperature T_c thermalizes the pointer around its equilibrium point at the rate κ_c . Work can be extracted coherently or incoherently from the excited spin by the demon's interrogation of the pointer position.

feedback scheme and sets precedence to the incorporation of thermal baths as a means of a realistic erasure or reset protocol.

Spin-boson model.— We consider a qubit with bare transition frequency Ω representing the working medium for heat-to-work conversion. A harmonic oscillator pointer of frequency ω couples to the qubit and is displaced to the left or right depending on the internal state of the qubit, see Fig. 1. The model Hamiltonian reads as

$$\begin{aligned} \hat{H} &= \frac{\hbar\Omega}{2}\hat{\sigma}_z + \hbar\omega\left(\hat{a}^\dagger\hat{a} + \frac{1}{2}\right) + \hbar\omega x_0\hat{\sigma}_z\frac{\hat{a} + \hat{a}^\dagger}{\sqrt{2}} \\ &= \frac{\hbar\Omega}{2}\hat{\sigma}_z + \hbar\omega\hat{b}^\dagger\hat{b} + \text{const}, \end{aligned} \quad (1)$$

with $\hat{\sigma}_z = |e\rangle\langle e| - |g\rangle\langle g|$, \hat{a} the oscillator's mode operator and $\hat{b} = \hat{a} + \hat{\sigma}_z x_0/\sqrt{2}$ the displaced mode operator. The Hamiltonian is found to be diagonal in the basis of qubit

state-dependent displaced Fock states,

$$\begin{aligned} |g, n_g\rangle &:= |g\rangle \otimes \hat{D}\left(\frac{x_0}{\sqrt{2}}\right) |n\rangle = |g\rangle \hat{D}|n\rangle, \\ |e, n_e\rangle &:= |e\rangle \otimes \hat{D}\left(-\frac{x_0}{\sqrt{2}}\right) |n\rangle = |e\rangle \hat{D}^\dagger |n\rangle, \end{aligned} \quad (2)$$

where the energy eigenvalues are $E_n^{e,g} = \pm \hbar\Omega/2 + \hbar\omega n$ modulo a constant, and $\hat{D}(\alpha) = \exp(\alpha\hat{a}^\dagger - \alpha^*\hat{a})$.

Let us discuss now the meaningful parameter regimes for the pointer. First, we work in the limit $\omega \ll \Omega$, in which the energy scales of the working medium and the pointer are separated and the pointer does not contribute appreciably to the energy balance of the engine.

The qubit-oscillator coupling strength has been expressed in terms of the state-dependent displacement $\pm x_0$ of the position quadrature $\hat{x} = (\hat{a} + \hat{a}^\dagger)/\sqrt{2}$, which also describes a shift of the qubit transition frequency by $\pm 2\omega x_0^2$. For sufficiently large x_0 , the pointer states become ‘‘macroscopically distinguishable’’ through their spatial separation [21, 23]. A demon would be functional so long as it possesses the ability to resolve this separation. This is unlike the case of a finite-dimensional pointer (e.g. a qubit), whose states would not remain distinguishable in the presence of noise. Furthermore, if the demon is able to measure a qubit, it could measure the system directly and the pointer would be redundant [27].

Besides the unitary dynamics, we now describe the roles of the hot and cold thermal reservoirs. The qubit is coupled to a hot thermal reservoir where heat flow is mediated by dissipators

$$\begin{aligned} \mathcal{L}_h\rho &= \sum_k \kappa_h(\Omega + k\omega) \left\{ [\bar{n}_h(\Omega + k\omega) + 1] \right. \\ &\quad \times \mathcal{D} \left[\sum_n d_{n,-k}^* |g, (n-k)_g\rangle \langle e, n_e| \right] \rho \\ &\quad \left. + \bar{n}_h(\Omega + k\omega) \mathcal{D} \left[\sum_n d_{n,k} |e, (n+k)_e\rangle \langle g, n_g| \right] \rho \right\}, \end{aligned} \quad (3)$$

with $\mathcal{D}[\hat{A}]\rho = \hat{A}\rho\hat{A}^\dagger - \{\hat{A}^\dagger\hat{A}, \rho\}/2$ and coefficients $d_{n,k} = \langle n|\hat{D}^2|n+k\rangle$, derived from secular approximation of the weak coupling master equation, see App. A.

The cold reservoir is not coupled to the qubit, but to the pointer: it takes care of erasing the information stored in it, through a continuous coupling with the displaced mode operator \hat{b} described by the dissipators [28]

$$\mathcal{L}_c\rho = \kappa_c(\bar{n}_c + 1)\mathcal{D}[\hat{b}]\rho + \kappa_c\bar{n}_c\mathcal{D}[\hat{b}^\dagger]\rho. \quad (4)$$

In the case where the displacement from equilibrium x_0 is greater than the thermal width $x_{\text{th}} = \coth^{1/2} \hbar\omega/2k_B T_c$, i.e. when the pointer positions for the two qubit states are distinct, the overall time evolution governed by Eqs. (1)-(4) brings the system to an approximate mixed steady state of the form

$$\rho_\infty \approx (1 - p_\infty)|g\rangle\langle g| \otimes \hat{D}\rho_g\hat{D}^\dagger + p_\infty|e\rangle\langle e| \otimes \hat{D}^\dagger\rho_e\hat{D}. \quad (5)$$

In particular, when the hot thermal contact is weak, $\kappa_h \ll \kappa_c$, we have $p_\infty \approx \bar{n}_h/(2\bar{n}_h + 1)$ and $\rho_{e,g} \approx \exp(-\hbar\omega\hat{a}^\dagger\hat{a}/k_B T_c)/Z_c$ to lowest order, i.e. a T_h -thermal mixture of displaced T_c -thermal pointer states encoding the qubit state.

Having set the model, we consider two variants of work extraction by a demon: an active control agent performing random measurement-feedback operations, and a coherent control field continuously monitoring the pointer.

Random measurement-feedback scheme.— An active demon would interrogate the pointer position and perform necessary feedback operations based on the measurement outcome. We shall consider the following measurement-feedback protocol occurring at a rate γ : (i) a dichotomic projective measurement (\hat{P} and $1 - \hat{P}$) of the pointer to detect whether it is on the left ($\langle \hat{x} \rangle < 0$), followed by (ii) work extraction via a Rabi flip $\hat{\sigma}_x$ induced by a strong control pulse if the pointer is on the left, i.e. the qubit is most probably excited. For sufficiently sparse Poisson-distributed events, the process can be effectively described by the coarse-grained generator [29–32]

$$\mathcal{L}_m\rho = \gamma\mathcal{D}[\hat{\sigma}_x\hat{P}]\rho + \gamma\mathcal{D}[\hat{P}]\rho, \quad (6)$$

assuming an ideal feedback mechanism at infinitesimally short times. In order to minimize the demon’s invasive influence on the pointer, the interrogation rate should be lower than the damping rate of the pointer, $\gamma \ll \kappa_c$.

Ideally, the demon would be able to generate a maximum energy output of $W_{\text{max}} = \hbar(\Omega - 2\omega x_0^2)p_\infty$ per interrogation, assuming vanishing overlap between the two displaced pointer states in (5). In fact, such an intuitive scheme is sufficient for extracting energy close to the ergotropy [33] contained in the state (5), $W_{\text{erg}} \approx \hbar(\Omega - \omega)p_\infty - \hbar\omega\bar{n}_c$, which eliminates the need for a cyclic unitary operation that would most likely require a non-trivial implementation.

Alternatively, measurements could also be described by POVMs with a smooth position dependence, as could be obtained e.g. from position-dependent exchange interactions with a stream of ancillary qubits extracting the excitation [24, 26].

The present scheme is autonomous in the sense that it does not rely on externally imposed engine strokes with synchronized switching of control pulses or couplings to thermal reservoirs. The random measurement process not only facilitates a convenient assessment of stationary energy flows, $\dot{Q}_{c,h,m} = \text{tr}\{\hat{H}\mathcal{L}_{c,h,m}\rho_\infty\}$, but it also does not depend on the precise timing of ‘‘measurement strokes’’. Note that even though we model the overall effect of the control operations on the system state by a dissipative channel \mathcal{L}_m , the corresponding change in steady-state energy contains both heat input and work output. Specifically, $\dot{Q}_m = \dot{Q}_{\text{ba}} - \dot{W}$, where \dot{W} denotes the output power extracted via the feedback control pulse, and \dot{Q}_{ba} accounts for the effective increase in entropy due to the measurement back-action on the pointer, more commonly interpreted as a form of ‘‘quantum heat’’ [9]. More

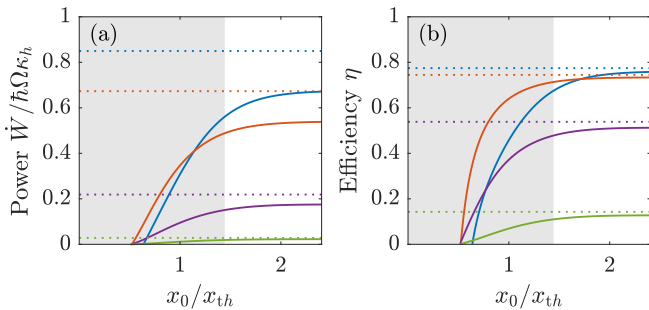


FIG. 2. Steady-state output power (a) and efficiency (b) against cold bath temperature expressed in terms of the thermal width x_{th} of the pointer (zero temperature on the right). The blue, red, purple, and green curves correspond to measurement rates $\gamma/\omega = 10^{-1}$, 10^{-2} , 10^{-3} , and 10^{-4} , respectively. The horizontal dotted lines represent the approximations γW_{max} and (8), the shaded region marks where $\bar{n}_c \geq \bar{n}_h$. We fix $\Omega = 100\omega$, $x_0 = 2.5$, $\kappa_h = 10^{-3}\omega$, $\kappa_c = 0.1\omega$, $\bar{n}_h = 1$.

explicitly, \hat{Q}_{ba} can be re-expressed in terms of a unital (or entropy-increasing) channel $\hat{Q}_{\text{ba}} = 2\gamma\hbar\omega \text{tr}\{\hat{b}^\dagger\hat{b}\mathcal{D}[\hat{P}]\rho_\infty\}$, which describes the pure pointer measurement without feedback in the protocol.

The output power is given by the average excitation energy of the qubit contained in the post-measurement state,

$$\dot{W} = \gamma \text{tr} \left\{ \hat{P} \rho_\infty \hat{P} [\hbar\Omega + 2\hbar\omega x_0 \hat{x}] \hat{\sigma}_z \right\}. \quad (7)$$

When the measurement rate $\gamma \ll \kappa_c$ and the pointer separation $x_0 \gg 1$, the projector would reduce the state to the excited branch in (5) resulting in the benchmark power γW_{max} . The repeated measurements however diminish the branch weight, $p_\infty \approx \bar{n}_h / (2\bar{n}_h + 1 + \gamma/\kappa_h)$, see App. A. For the efficiency, $\eta = \dot{W}/\hat{Q}_h$, we find the approximate upper bound

$$\eta_{\text{max}} \approx \frac{1 - 2\omega x_0^2/\Omega}{1 + 2[1 + (2\bar{n}_h + 2)\kappa_h/\gamma]\omega x_0^2/\Omega}. \quad (8)$$

Both the output power and efficiency grow with γ until an optimum is reached around $\gamma \lesssim \kappa_c$. At higher rates, the repeated measurements would effectively freeze the pointer dynamics.

For simplicity and numerical stability in our simulations, we now consider the measurement by a projection onto a finite subspace of left-displaced Fock states, $\hat{P} = \sum_{n=0}^N \hat{D}^\dagger |n\rangle\langle n| \hat{D}$. Here, the cutoff N is chosen such that the included pointer levels contain at least the ground state, but otherwise do not exceed the potential energy of the left-displaced oscillator at $x = 0$, i.e. $2N + 1 \leq \max\{x_0^2, 1\}$. This should be comparable in effect to an ideal position measurement $\hat{P}_x = \int_{-\infty}^0 dx |x\rangle\langle x|$ in the envisaged operation regime $x_0 \gg x_{\text{th}}$, while avoiding convergence issues due to discontinuities in position representation.

Figure 2 shows (a) the output powers and (b) efficiencies as a function of T_c for various rates γ . Here, T_c is expressed in terms of the ratio between pointer displacement x_0 and characteristic thermal width $x_{\text{th}} \geq 1$. This is an exemplary case where $x_0 = 2.5$, which should lead to a clear separation of the ground- and excited-state distributions so long as the cold bath temperature is sufficiently low ($x_0 > x_{\text{th}}$). In fact, in this low-temperature limit, the efficiencies approach the analytical benchmarks given by (8). The actual output powers, however, fall below the benchmark value γW_{max} as γ increases.

At high temperatures, the model stops working and the output power becomes negative due to the larger overlap between the two displaced thermal states, which leads to inaccurate readout of the qubit state. Moreover, we see in Fig. 2 that low measurement rates will decrease the output. The optimum is reached when γ approaches κ_c (blue curves). Further simulations reveal that greater γ will make it worse again; this amounts to a Zeno limit where the frequent measurement hinders the pointer from moving between the left and the right equilibrium.

At vanishing κ_h , the efficiency in (8) would not exceed the Otto efficiency, $\eta \approx 1 - 4x_0^2\omega/\Omega < 1 - \omega/\Omega = \eta_{\text{Otto}}$. However, this engine is not an Otto engine in the typical sense. We see in Fig. 2 (shaded region) that the engine operates outside the standard Otto operation window ($\omega/\Omega > T_c/T_h$, i.e. $\bar{n}_h > \bar{n}_c$), albeit at lower output power and efficiency. In fact, this wider operation window is a manifestation of using a mechanical pointer with “macroscopically distinguishable” states. If it were replaced by a qubit pointer, operation would be restricted to the Otto window $\bar{n}_h > \bar{n}_c$, because measurement errors leading to work consumption instead of extraction would proliferate with growing \bar{n}_c and the net work output per interrogation would be limited by $\hbar(\Omega - \omega)(\bar{n}_h - \bar{n}_c)/(2\bar{n}_h + 1)(2\bar{n}_c + 1)$, regardless of the system-pointer interaction strength [34].

Even though the maximum efficiency does not reach η_{Otto} (0.99 in this case), such a demon engine has its advantages over standard Otto engines where a trade-off between efficiency and work output is inevitable and η_{Otto} is attainable only in the limiting scenario of vanishing work output [35].

Integrated demon scheme.— Instead of an incoherent scheme based on random monitoring by an external agent, it would be insightful to formulate an integrated setup in which the measurement-feedback takes place internally and all energy exchanges become transparent. To this end, we consider a position-dependent driving field of strength ζ with detuning Δ , which now plays the role of the demon that probes the qubit in a non-invasive, coherent manner. We can describe the effect of such a demon by a time-dependent Rabi term

$$\hat{V}(t) = \hbar\zeta f(\hat{x}) e^{-i(\Omega - \Delta)t} |e\rangle\langle g| + h.c., \quad (9)$$

which serves as an interface for work extraction depending on the position-dependent function $f(\hat{x})$. Possible choices of $f(x)$ include a Heaviside function $\Theta(-x)$ or a

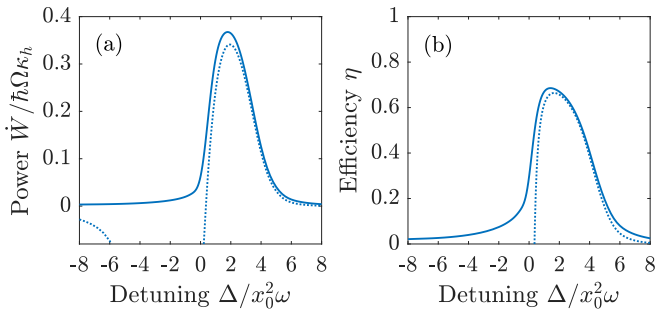


FIG. 3. Output power (a) and efficiency (b) against the detuning Δ of the driving field for $f(x) = \Theta(-x)$ (solid) and $f(x) = 1$ (dotted). We fix $\Omega = 100\omega$, $x_0 = 2.5$, $\kappa_h = 10^{-3}\omega$, $\kappa_c = 0.1\omega$, $\zeta = 0.1\omega$ and the same hot and cold bath occupancy $\bar{n}_c = \bar{n}_h = 1$.

Gaussian centred around $x = -x_0$.

To assess the scheme's steady-state performance, we consider the weak driving limit, $\zeta \ll \omega, \Omega$, where corrections to the thermal dissipators $\mathcal{L}_{h,c}$ can be omitted [36, 37]. In the frame rotating at the driving frequency, the time dependence due to (9) conveniently disappears and the time evolution follows from $\tilde{\mathcal{L}}_{h,c} = \mathcal{L}_{h,c}$ and $\tilde{H}/\hbar = \Delta\hat{\sigma}_z/2 + \omega\hat{b}^\dagger\hat{b} + \zeta f(\hat{x})\hat{\sigma}_x$. The corresponding steady state $\tilde{\rho}_\infty$ describes the engine's limit cycle and yields the average output power [38]

$$\dot{W} = -\text{tr} \left\{ \rho_\infty(t) \partial_t \hat{V}(t) \right\} = -\hbar\zeta(\Omega - \Delta) \text{tr} \left\{ f(\hat{x}) \hat{\sigma}_y \tilde{\rho}_\infty \right\}. \quad (10)$$

The heat fluxes from the hot and cold reservoirs read as

$$\dot{Q}_{h,c} = \text{tr} \left\{ \left[\hat{H} + \hbar \frac{\Omega - \Delta}{2} \hat{\sigma}_z \right] \mathcal{L}_{h,c} \tilde{\rho}_\infty \right\}. \quad (11)$$

Figure 3 shows the engine's output powers and efficiencies at its limit cycle as a function of the detuning for an exemplary set of engine parameters and various cold bath temperatures. Here, the optimal output power is much smaller than the driving rate times the extractable excitation energy, $\zeta W_{\max} \approx 29\hbar\Omega\kappa_h$. This was not the case for the previously discussed incoherent measurement-feedback scheme, which exhibits a work power of up to γW_{\max} , because that scheme implicitly assumes a large driving strength and short feedback time such that the feedback is essentially described by a conditional spin flip depending on the position of the pointer. In the current scheme, the driving field would not cause a full spin flip. Nevertheless, the output power can be comparable to what the measurement-feedback scheme predicts for similar settings, see also Fig. 4.

Here, we achieve a maximum work power (and efficiency) when $\Delta \approx 2\omega x_0^2$. This is because the frequency of the qubit is modulated by the pointer position, and at this driving frequency, the field addresses predominantly the qubit only when the pointer is located at $-x_0$, i.e. the qubit is excited and the field is able to extract a positive net energy from it. Hence one can modify the

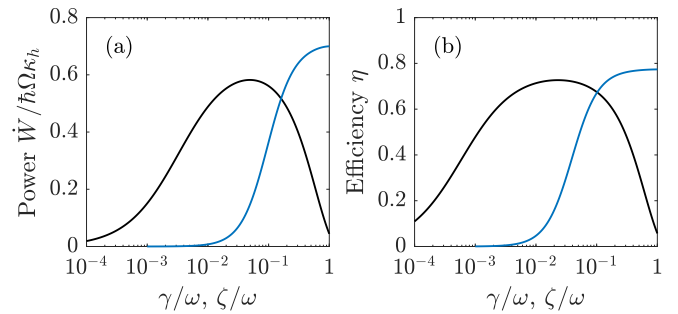


FIG. 4. Output power (a) and efficiency (b) against the rate γ or ζ , comparing the measurement-feedback scheme (black) with the integrated scheme (blue) at optimal detuning $\Delta = 2\omega x_0^2$ and $f(x) = \Theta(-x)$. The other parameters are taken from Fig. 3. Note that underlying master equation model may no longer be reliable for $\zeta \sim \omega$.

scheme by removing the position dependence $f(x)$ and consider a non-invasive interrogation of the qubit state solely through the application of a red-detuned field of $\Delta \approx 2\omega x_0^2$. This does not cause a backaction-induced direct flow of energy to the pointer, a minor contribution to the energy balance when $\Omega \gg \omega$, which is inherent to the position-dependent case and appears explicitly as \dot{Q}_{ba} in the previous measurement-feedback scheme.

The dotted line in Fig. 3 shows the output power and efficiency achievable by non-invasive interrogation as a function of the detuning. Close to the optimal working point, the performance is almost the same as the position-dependent case, but the position-independent driving will cease to produce work as the detuning approaches zero; indeed, we would obtain a heat pump *consuming* work at negative detunings.

Finally, Figure 4 compares the random measurement-feedback scheme with the integrated scheme at optimal detuning and position-dependent driving in terms of their powers and efficiencies. We plot them as a function of the respective interrogation rates γ and ζ . The former scheme performs well over a broad range of small measurement rates γ , but it stops working when the Zeno effect kicks in at $\gamma > \kappa_c$. The integrated scheme eventually catches up at strong driving rates ζ .

Conclusion & outlook.— We have presented a self-contained engine model in which useful energy is extracted from thermal excitations of a quantum spin by a handicapped Maxwell demon. It is allowed to interrogate the spin state only indirectly, by inquiring the position of a macroscopic mechanical pointer attached to the spin. While this comes at the cost of measurement backaction, mechanical damping from a cold thermal reservoir stabilizes the pointer and alleviates the need for an explicit Landauer erasure protocol upon extraction. We studied the engine performance both for an active demon performing measurement-feedback events at random times and for an integrated demon in the form of a stationary control field. Both cases can operate at simultaneously high output power and efficiency, and also outside

the thermal operation window of typical quantum Otto engines, which puts forth the paradigm of continuous measurement-driven engines.

Regarding implementations, a suitable experimental platform for the presented model can be found in molecular batteries [39]: molecules with an optical electronic transition strongly coupled to an infrared vibration mode. In fact, the spin-boson Hamiltonian (1) resembles the Holstein Hamiltonian for a molecule undergoing fast vibrational relaxation [40]. Displacements can reach magnitudes $x_0 \sim 1$, while the vibrational relaxation time is short compared to the optical lifetime, i.e. $\kappa_h \ll \kappa_e$.

A broadband optical light source (e.g. filtered sunlight) could serve as the hot bath exciting the electron, and a resonant IR cavity mode could be employed to monitor the vibration mode displacement [41, 42]. Alternatively, our scheme could be realized in a tailored trapped-ion setup similar to the recently demonstrated spin-flywheel engine [43].

Acknowledgments.—The authors acknowledge fruitful discussions with Robert Alicki and Claudiu Genes. This research is supported by the National Research Fund and the Ministry of Education, Singapore, under the Research Centres of Excellence programme.

-
- [1] M. O. Scully, M. S. Zubairy, G. S. Agarwal, and H. Walther, *Science* **299**, 862 (2003).
- [2] M. O. Scully, *Phys. Rev. Lett.* **104**, 207701 (2010).
- [3] M. O. Scully, K. R. Chapin, K. E. Dorfman, M. B. Kim, and A. Svidzinsky, *Proc. Natl. Acad. Sci.* **108**, 15097 (2011).
- [4] R. Uzdin, *Phys. Rev. Applied* **6**, 024004 (2016).
- [5] J. Klatzow, J. N. Becker, P. M. Ledingham, C. Weinzel, K. T. Kaczmarek, D. J. Saunders, J. Nunn, I. A. Walmesley, R. Uzdin, and E. Poem, *Phys. Rev. Lett.* **122**, 110601 (2019).
- [6] J. Roßnagel, O. Abah, F. Schmidt-Kaler, K. Singer, and E. Lutz, *Phys. Rev. Lett.* **112**, 030602 (2014).
- [7] G. Manzano, F. Galve, R. Zambrini, and J. M. R. Parrondo, *Phys. Rev. E* **93**, 052120 (2016).
- [8] J. Klaers, S. Faelt, A. Imamoglu, and E. Togan, *Phys. Rev. X* **7**, 031044 (2017).
- [9] C. Elouard, D. A. Herrera-Martí, M. Clusel, and A. Auffèves, *npj Quantum Inf.* **3**, 9 (2017).
- [10] C. Elouard and A. N. Jordan, *Phys. Rev. Lett.* **120**, 260601 (2018).
- [11] L. Buffoni, A. Solfanelli, P. Verrucchi, A. Cuccoli, and M. Campisi, *Phys. Rev. Lett.* **122**, 070603 (2019).
- [12] C. Elouard, M. Waegell, B. Huard, and A. N. Jordan, *arXiv:1904.09289* (2019).
- [13] D. Mandal and C. Jarzynski, *Proc. Natl. Acad. Sci.* **109**, 11641 (2012).
- [14] A. C. Barato and U. Seifert, *Europhys. Lett.* **101**, 60001 (2013).
- [15] P. Strasberg, G. Schaller, T. Brandes, and M. Esposito, *Phys. Rev. Lett.* **110**, 040601 (2013).
- [16] J. M. Horowitz and M. Esposito, *Phys. Rev. X* **4**, 031015 (2014).
- [17] J. V. Koski, A. Kutvonen, I. M. Khaymovich, T. Ala-Nissila, and J. P. Pekola, *Phys. Rev. Lett.* **115**, 260602 (2015).
- [18] J. V. Koski and J. P. Pekola, “Quantum thermodynamics in a single-electron box,” in *Thermodynamics in the Quantum Regime*, edited by F. Binder, L. A. Correa, C. Gogolin, J. Anders, and G. Adesso (Springer, Cham, 2018) pp. 897–915.
- [19] C. Elouard, D. Herrera-Martí, B. Huard, and A. Auffèves, *Phys. Rev. Lett.* **118**, 260603 (2017).
- [20] A. Aydin, A. Sisman, and R. Kosloff, *arXiv:1908.04400* (2019).
- [21] R. Alicki, *arXiv:1305.4910* (2013).
- [22] P. Faist, F. Dupuis, J. Oppenheim, and R. Renner, *Nat. Commun.* **6**, 7669 (2015).
- [23] R. Alicki and M. Horodecki, *J. Phys. A: Math. Theor.* **52**, 204001 (2019).
- [24] P. Strasberg, G. Schaller, T. Brandes, and M. Esposito, *Phys. Rev. X* **7**, 021003 (2017).
- [25] P. Strasberg, *arXiv:1810.00698* (2018).
- [26] S. Seah, S. Nimmrichter, and V. Scarani, *Phys. Rev. E* **99**, 042103 (2019).
- [27] G. Sewell, in *AIP Conference Proceedings*, Vol. 962 (AIP, 2007) pp. 215–222.
- [28] Eq. (4) can be obtained from the usual Born-Markov secular approximation [29, 39], assuming an oscillator bath linearly coupled to the \hat{x} -quadrature. This would also result in an additional pure dephasing term $\propto \mathcal{D}[\hat{\sigma}_z]\rho$, which however scales with the bath spectral density at zero frequency and is thus often negligible.
- [29] H.-P. Breuer and F. Petruccione, *The Theory of Open Quantum Systems* (Oxford University Press, 2002).
- [30] K. Hornberger, *Europhys. Lett.* **77**, 50007 (2007).
- [31] H. M. Wiseman and G. J. Milburn, *Quantum Measurement and Control* (Cambridge University Press, 2009).
- [32] K. Jacobs, *Quantum Measurement Theory and its Applications* (Cambridge University Press, Cambridge, 2014).
- [33] A. E. Allahverdyan, R. Balian, and T. M. Nieuwenhuizen, *Europhys. Lett.* **67**, 565 (2004).
- [34] S. Lloyd, *Phys. Rev. A* **56**, 3374 (1997).
- [35] R. Kosloff and Y. Rezek, *Entropy* **19**, 136 (2017).
- [36] H. J. Carmichael, *Statistical Methods in Quantum Optics I* (Springer, Berlin, Heidelberg, 1999).
- [37] K. Szczygielski, D. Gelbwaser-Klimovsky, and R. Alicki, *Phys. Rev. E* **87**, 012120 (2013).
- [38] R. Alicki, *J. Phys. A: Math. Gen.* **12**, L103 (1979).
- [39] R. Alicki, *J. Chem. Phys.* **150**, 214110 (2019).
- [40] M. Reitz, C. Sommer, and C. Genes, *Phys. Rev. Lett.* **122**, 203602 (2019).
- [41] J. P. Long and B. S. Simpkins, *ACS Photonics* **2**, 130 (2015).
- [42] A. Shalabney, J. George, J. Hutchison, G. Pupillo, C. Genet, and T. W. Ebbesen, *Nat. Commun.* **6**, 5981 (2015).
- [43] D. von Lindenfels, O. Gräß, C. T. Schmiegelow, V. Kaushal, J. Schulz, M. T. Mitchison, J. Goold, F. Schmidt-Kaler, and U. G. Poschinger, *Phys. Rev. Lett.* **123**, 080602 (2019).

Appendix A: Validity of the hot bath dissipator

Here we compare the local and global secular form of the hot bath dissipator that arises in the usual manner from a linear exchange interaction of the qubit with a thermal oscillator bath. For the local model, one simply employs the standard dissipator for an isolated qubit,

$$\mathcal{L}_h^{\text{loc}} \rho = \kappa_h(\Omega)[\bar{n}_h(\Omega) + 1]\mathcal{D}[\hat{\sigma}_-]\rho + \kappa_h(\Omega)\bar{n}_h(\Omega)\mathcal{D}[\hat{\sigma}_+]\rho, \quad (\text{A1})$$

assuming that the qubit-pointer coupling and thus the influence of the pointer on the qubit energy are negligible. For an isolated qubit, the jump operators $\hat{\sigma}_\pm$ can mediate only a single transition of frequency Ω , given the thermal coupling rate κ_h and the mean thermal bath occupation \bar{n}_h at this frequency. In the combined qubit-pointer system, the same operators now induce a family of transitions $\Omega + k\omega$ with $k \in \mathbb{Z}$. Specifically, we can expand in terms of the combined energy basis (2),

$$\hat{\sigma}_+ = |e\rangle\langle g| = \sum_{m,n=0}^{\infty} \langle m|\hat{D}^2|n\rangle |e, m_e\rangle\langle g, n_g| = \sum_{n=0}^{\infty} \sum_{k=-n}^{\infty} \underbrace{\langle n+k|\hat{D}^2|n\rangle}_{\equiv d_{n,k}} |e, (n+k)_e\rangle\langle g, n_g|, \quad (\text{A2})$$

with the weight coefficients $d_{n,k}$. The above local dissipator contains cross-terms between different transitions $k \neq k'$, which means that it preserves a certain amount of coherences between different energy levels of the system. Moreover, using it implies that one can neglect the frequency dependence of the bath parameters, $\kappa_h(\Omega + k\omega) \approx \kappa_h$ and $\bar{n}_h(\Omega + k\omega) \approx \bar{n}_h$, which is only valid when $\Omega \gg \omega$.

The global secular model does not preserve any coherences between different Fock numbers, because it contains only resonant jump terms,

$$\begin{aligned} \mathcal{L}_h^{\text{glo}} \rho &= \sum_k \kappa_h(\Omega + k\omega) [\bar{n}_h(\Omega + k\omega) + 1] \mathcal{D} \left[\sum_n d_{n,-k}^* |g, (n-k)_g\rangle\langle e, n_e| \right] \rho \\ &+ \sum_k \kappa_h(\Omega + k\omega) \bar{n}_h(\Omega + k\omega) \mathcal{D} \left[\sum_n d_{n,k} |e, (n+k)_e\rangle\langle g, n_g| \right] \rho. \end{aligned} \quad (\text{A3})$$

For the demon models studied in the main text, we find that both dissipators yield approximately the same results. The reason is, on the one hand, that we indeed consider $\Omega \gg \omega$ and can thus assume constant κ_h and \bar{n}_h . On the other hand, our model also includes a cold bath with stronger damping rate $\kappa_c > \kappa_h$, which suppresses any coherences between Fock states of the pointer that $\mathcal{L}_h^{\text{loc}}$ alone would have preserved.

The steady-state heat input for $\kappa_h \ll \kappa_c$ can then be approximated using the local dissipator, too,

$$\dot{Q}_h \approx \text{tr} \left\{ \left(\frac{\hbar\Omega}{2} + \hbar\omega x_0 \hat{x} \right) \hat{\sigma}_z \mathcal{L}_h^{\text{loc}} \rho_\infty \right\} \approx \hbar\kappa_h [\bar{n}_h(1 - p_\infty)(\Omega + 2\omega x_0^2) - (\bar{n}_h + 1)p_\infty(\Omega - 2\omega x_0^2)]. \quad (\text{A4})$$

For the qubit excitation probability, the same approximation yields

$$\begin{aligned} \partial_t p_e(t) &\approx \text{tr} \{ |e\rangle\langle e| (\mathcal{L}_h^{\text{loc}} + \mathcal{L}_m) \rho \} = -\kappa_h(\bar{n}_h + 1)p_e(t) + \kappa_h\bar{n}_h[1 - p_e(t)] - \gamma \text{tr} \{ \hat{\sigma}_z \hat{P} \rho \hat{P} \} \\ &\approx -\kappa_h(\bar{n}_h + 1)p_e(t) + \kappa_h\bar{n}_h[1 - p_e(t)] - \gamma p_e(t). \end{aligned} \quad (\text{A5})$$

Here the second line holds in the ideal operation regime of $\gamma \ll \kappa_c$ and $x_0 \gg 1$, when \hat{P} reduces the state to its excited branch. At steady state, we obtain $p_\infty = p_e(\infty) = \bar{n}_h/(2\bar{n}_h + 1 + \gamma/\kappa_h)$, as used in the main text.